

UWL REPOSITORY
repository.uwl.ac.uk

Effects of bone damage on creep behaviours of human vertebral trabeculae

O'Callaghan, Paul, Szarko, Matthew, Wang, Yue and Luo, Jin ORCID: <https://orcid.org/0000-0001-5451-9535> (2017) Effects of bone damage on creep behaviours of human vertebral trabeculae. *Bone*, 106. pp. 204-210. ISSN 8756-3282

<http://dx.doi.org/10.1016/j.bone.2017.10.022>

This is the Accepted Version of the final output.

UWL repository link: <https://repository.uwl.ac.uk/id/eprint/6898/>

Alternative formats: If you require this document in an alternative format, please contact: open.research@uwl.ac.uk

Copyright: Creative Commons: Attribution-Noncommercial-No Derivative Works 4.0

Copyright and moral rights for the publications made accessible in the public portal are retained by the authors and/or other copyright owners and it is a condition of accessing publications that users recognise and abide by the legal requirements associated with these rights.

Take down policy: If you believe that this document breaches copyright, please contact us at open.research@uwl.ac.uk providing details, and we will remove access to the work immediately and investigate your claim.

1 **Effects of bone damage on creep behaviours of human vertebral trabeculae**

2
3 Paul O’Callaghan PhD¹, Matthew Szarko PhD², Yue Wang MD, PhD^{3*}, Jin Luo PhD^{1*}

4
5
6 ¹School of Applied Sciences, London South Bank University, London SE1 0AA, UK

7 ²Institute of Medical and Biomedical Education, St George’s University of London, London
8 SW17 0RE, UK (Present address: Division of Surgery and Interventional Science, University
9 College London, London, NW3 2QG, UK)

10 ³Spine lab, Department of Orthopedic Surgery, The First Affiliated Hospital, College of
11 Medicine, Zhejiang University, Hangzhou, PR China

12
13 Correspondence to Dr Jin Luo, School of Applied Sciences, London South Bank University,
14 103 Borough Road, London SE1 0AA, UK Tel: 020 78157941, Email: luoj4@lsbu.ac.uk **OR**
15 Dr Yue Wang, Spine lab, Department of Orthopedic Surgery, The First Affiliated Hospital,
16 College of Medicine, Zhejiang University, Hangzhou, PR China, Tel: 86 571 87236128,
17 Email: wangyuespine@zju.edu.cn or wangyuespine@gmail.com

Abstract

A subgroup of patients suffering with vertebral fractures can develop progressive spinal deformities over time. The mechanism underlying such clinical observation, however, remains unknown. Previous studies suggested that creep deformation of the vertebral trabeculae may play a role. Using the acoustic emission (AE) technique, this study investigated effects of bone damage (modulus reduction) on creep behaviours of vertebral trabecular bone. Thirty-seven human vertebral trabeculae samples were randomly assigned into five groups (A to E). Bones underwent mechanical tests using similar experimental protocols but varied degree of bone damage was induced. Samples first underwent creep test (static compressive stress of 0.4 MPa) for 30 minutes, and then were loaded in compression to a specified strain level (0.4%, 1.0%, 1.5%, 2.5%, and 4% for group A to E, respectively) to induce different degrees of bone damage (0.4%, no damage control; 1.0%, yield strain; 1.5%, beyond yield strain, 2.5% and 4%, post-ultimate strains). Samples were creep loaded (0.4 MPa) again for 30 minutes. AE techniques were used to monitor bone damage. Bone damage increased significantly from group A to E ($P < 0.05$), with more than 30% of modulus reduction in group D and E. Before compressive loading, creep deformation was not different among the five groups and AE hits in creep test were rare. After compressive loading, creep deformation was significantly greater in group D and E than those in other groups ($P < 0.05$). The number of AE hits and other AE measurements during creep test were significantly greater in group D and E than in group A, B, and C ($P < 0.05$ for all). Data suggested that with the increase of vertebral trabecular bone damage, substantial creep deformation may occur even when the vertebra was under physiological loads. The boosted creep deformation observed may be attributed to newly created trabecular microfractures. Findings provide a possible explanation as to why some vertebral fracture patients develop progressive spinal deformity over time.

Key words: vertebral fracture; creep; trabeculae; mechanical test; biomechanics

1 Introduction

Vertebral compression fracture is one of the most common fractures in the elderly [1] and often causes back pain and other symptoms that need clinical treatment. As the world's older population grows, healthcare costs for vertebral compression fracture have increased continuously [2]. Although most patients with vertebral compression fracture have favourable clinical outcomes after appropriate treatments, there is a subgroup of patients who developed progressive vertebral collapse over time, resulting in disabling back pain, spinal deformity, or even neurological complications [3, 4]. It is hence important to identify these patients for preventive clinical interventions. To date, however, a screening tool to identify vertebral fracture patients who are at risk of progressive vertebral collapse and deformity is absent [5]. This is partly due to the limited understanding on the determinants of progressive vertebral collapse that followed vertebral fracture.

Previous studies have revealed that under physiological load a vertebra may continue to deform in a "creep" process [6]. Creep deformation is partially irreversible and may contribute to progressive spinal deformity. Further experiments observed that the speed of creep deformation may associate with the degree of vertebra damage [7]. In theory, creep in some fractured vertebrae may be accelerated to such an extent that vertebral collapse, a severe consequence of creep, occurs. Yet, a clear quantitative relationship between the degree of bone damage and vertebral creep deformation remained undetermined. Although vertebral components, including trabecular bone, cortical shell and endplate, all contribute to vertebral creep deformation, trabecular bone plays a dominant role [8, 9]. Studies on creep behaviour of vertebral trabecular bone, therefore, can provide important information on vertebral creep.

The mechanism underlying bone creep is not fully understood, though some studies suggested that it may relate to bone viscoelasticity and bone damage accumulation [10-12].

The acoustic emission (AE) technique is a non-invasive and non-destructive approach used to monitor the integrity of engineering materials. This technique is based on the phenomenon that a material under an external load will produce sound (AE signal) when it starts to fail, such as the cracking noise from a broken tree when it falls. As a well-developed damage-monitoring technique, AE has been used in studies of cortical [13-16] and cancellous bones [17, 18]. Yet, the AE technique has not been used to study vertebral creep.

Using the AE technique to monitor the creep behaviours of vertebral trabeculae, the current study aims to determine the relationship between bone damage and creep deformation in human vertebral trabeculae.

2 Materials and Methods

2.1 Experiment design

Thirty-seven cylindrical trabecular bone samples from human thoracic or lumbar vertebrae were randomly assigned to 5 groups (group A - E). All bone samples used the same experimental protocols but different levels of damage loading. First, trabecular samples underwent creep loading (static compressive stress of 0.4 MPa) for 30 minutes. Then, the load was removed for 30 minutes to allow for recovery. Following recovery, samples in each group were loaded in compression to a specified strain (0.4% in group A; 1.0% in group B; 1.5% in group C; 2.5% in group D and 4% in group E) to induce bone damage. Finally, the samples were creep loaded (0.4 MPa) again for an additional 30 minutes.

2.2 Specimens

Five human spines (3 men and 2 women) donated for medical research were obtained from Science Care (USA). The donors were 36 to 73 years old (mean 57 years), with no known history of disease involving bone metabolism. Materials were stored at -20°C till test. Each spine was thawed at 3°C and T8 to L5 vertebrae were dissected for study. Each vertebra underwent fluoroscopy and only those integral vertebrae without suspicious pathology were included. As a result, 43 vertebrae were obtained, from which 21 were randomly selected for the current study (**Table 1**).

Cylinder cores of trabecular bone were obtained from each vertebra using an 8mm external diameter diamond coated hole saw (THK Diamond Tools, China). During coring, the vertebra was clamped firmly to ensure that the longitudinal axis of the sample was perpendicular to the vertebral endplate. Samples were cooled with phosphate-buffered saline (PBS) during drilling. After coring, bone samples were visually assessed for any presence of mechanical damage. Samples showing any sign of damage were discarded. For each vertebra,

typically 2 cylindrical bone samples (axial diameter 6.3mm, height 19.3-28.4mm) were obtained from left and right regions of the vertebral body. A third sample can be obtained from the middle region for some vertebrae of large size. Bone samples were sealed in plastic bags and stored at -20°C until required for testing. As a result, 37 cylindrical bone samples were obtained, which were randomly assigned to group A to E. There are 9 samples in group A (1 sample from spine #1, #4 and #5, 2 samples from spine #3, and 4 samples from spine #2), 8 in group B (1 sample from spine #1, 2 samples from spine #3 and #4, and 3 samples from spine #2), 7 in group C (1 sample from spine #3, #4 and #5, and 4 samples from spine #2), 6 in group D (1 sample from spine #1 and #3, and 4 samples from spine #2), and 7 in group E (1 sample from spine #4 and #5, 2 samples from spine #3, and 3 samples from spine #2).

2.3 Mechanical tests and AE measurement

The height and diameter of each sample was measured using a Vernier calliper. If necessary, a sample was shortened to keep the aspect ratio (height/ diameter) less than 4, as recommended, to minimise end artefacts in mechanical testing [19]. The sample was then press-fit into two custom-made stainless steel endcaps, and held in place with cyanoacrylate adhesive. A custom-made jig was used to ensure that both endcaps were in alignment with the longitudinal axis of the cylinder sample [20] so that only uniaxial loading would occur during mechanical testing.

The mechanical test was performed using a Mach-1TM material testing device (Biomomentum, Canada) equipped with a 100N load cell in a displacement resolution of 0.001 mm and a load resolution of 0.005 N. Load and displacement signals were sampled at 100 Hz. A custom-made testing chamber (70mm × 70mm × 45 mm) was fixed to the base plate of the testing device (**Figure 1**). The sample was placed in the centre of the testing chamber and pressed by

a flat-bottomed circular compression plate (20 mm in diameter). During testing, the chamber was filled with PBS solution at room temperature.

An AE sensor (R15UG, Mistras Group Ltd, UK; operating frequency 50-200 kHz) was attached to the testing chamber (**Figure 1**) using cyanoacrylate adhesive [21]. Prior to experimental setup, the operation and performance of the AE transducer was confirmed with a pencil lead break test using an acrylic rod as outlined in ASTM. E976-10 [22]. Before each testing period, pencil lead break test was performed to verify the integrity of AE measurement setup. AE signals from AE sensor were transferred to the AE channel of the USB AE node (Model 1283, Mistras Group Ltd, UK), and load signals from the testing machine were input to the parametric channel of the USB AE node interface. Both signals were sampled and processed by the USB AE node system, using the supporting software AEWIn (version E5.30).

AE signal is measured in the form of discrete acoustic waves. Each wave is induced by a release of elastic energy from bone damage, and is often called an AE hit or AE event (**Figure 2**). The gain for the pre-amplifier of AE channel was set at 40 dB, and the sample rate at 20 MHz. The threshold for AE channel was set at 40 dB and the band-pass analogue filter at 20 to 300 kHz to eliminate any false triggers and to filter out noise from the machine [23]. Timing parameters for AE channel (peak definition time, 50 μ s; hit definition time, 200 μ s; hit lockout time, 300 μ s) were set based on the previous pencil lead break test [15, 22]. Sampled data of AE hits were processed by AEWIn to extract AE signal features for each hit, including amplitude, counts, and duration (**Figure 2**). The load signal from the testing machine was sampled at 10 Hz by the parametric channel. Acquired AE data and load data were input to a PC for analysis.

2.4 Experiment protocol

2.4.1 Creep loading

Using the load-control mode (creep mode), bone samples were compressively loaded to 13 N within 5 seconds, and maintained for 30 minutes to induce creep. The samples were then unloaded for a period of 30 minutes to allow recovery. A creep load of 13 N generated 0.4 MPa compressive stress on bone samples. Our previous experiments [6, 7] revealed that 0.4 MPa compressive stress was the average compressive stress on vertebral trabecular bone when a spinal motion segment was subjected to 1000 N creep load. This amount of load is approximately equivalent to the physiological load in the lumbar spine when a person is in a standing posture [24].

2.4.2 Compressive loading

Bone samples were loaded in compression to one of the 5 levels of strain (0.4%, 1.0%, 1.5%, 2.5%, and 4%) at a constant strain rate of 0.04% per second. As 0.4% strain is within the elastic range of trabecular bone [25], it was used as a control to establish AE features of an intact vertebral sample during creep loading. Strains of 1.0% (approximately the yield strain of trabecular bone), 1.5% (above the yield strain but below the ultimate strain), 2.5% (post-ultimate strains), and 4% (post-ultimate strains) were used to simulate overloading conditions that may induce acute vertebral fracture in the spine [25].

After compressed to the assigned strain, samples were unloaded to zero stress, with the compression plate returning to its original position prior to the loading cycle. Then, the samples were immediately re-loaded (0.04% strain per second) to previous strain level to obtain data for bone damage analysis. Samples were then unloaded to zero stress till second creep loading.

2.4.3 Second Creep loading

Immediately after the compressive loading, samples again underwent creep loading test using the above-mentioned creep loading protocol. After the second creep loading, bone samples were sectioned out of the endcaps, sealed in plastic bag, and then stored at -20°C.

2.4.4 Apparent density of bone samples

Tested bone samples were thawed to room temperature and rinsed in detergent solution to remove residual bone marrow. Samples were then dried in room temperature for 24 hours. The mass and bulk volume were then measured to calculate apparent density (g/mm^3).

2.5 Data analysis

Load data and displacement data, as acquired by the testing machine, were used to calculate stress and strain (**Figure 3 and 4**). Strain was calculated in the unit of μstrain or percentage strain (1% strain = 10,000 μstrain). The strain measured in the first 5 seconds of creep test was treated as elastic strain, and was excluded from the calculation of creep strain. As reported previously [6, 7, 11, 26], the primary creep (T1, **Figure 4**) lasted approximately 2 to 3 minutes, with a high creep rate. The secondary creep (T2, **Figure 4**) lasted longer, and had a much lower creep rate. Creep strain in the primary creep was calculated as accumulated strain in the first 3-minute of creep test. Creep rate in the secondary creep was calculated between the 10th min and 20th minute of creep test using a linear regression model [11].

Signal features of AE hits in a certain period were analysed to acquire AE measurements, including cumulative hits, cumulative counts, cumulative duration, maximal and mean amplitude of AE hits. A MATLAB based program was used to compare the load data captured by the USB AE node and the testing device to eliminate time offset and synchronize related data.

Bone damage was calculated using the stress-strain curves obtained from compressive loading and re-loading. The Young's modulus was calculated as the slope of the best-fit

straight line between strains 0.1% and 0.4% of the stress-strain curve in the compressive loading circle [27]. The residual modulus was calculated as the slope of the approximately linear region in the compressive re-loading cycle [28]. Modulus reduction was calculated as the percentage difference between the Young's and residual modulus, and was used to reflect the degree of mechanical damage in vertebral sample [28].

2.6 Statistics

Mean (SD) and median (interquartile range, IQR) were used to depict various measurements, as appropriate. One-way ANOVA was used to compare apparent density and bone damage among groups. As other data were not in normal distribution, non-parametric statistics, including Kruskal-Wallis test and Mann-Whitney U test, were used in comparison. To examine effect of donor on creep deformation, creep data were log transformed and analysed using two-way ANOVA, with experimental group as fixed factor and donor as random factor. Non-parametric correlation analysis (Kendall's τ) was used to examine the relationship between creep deformation and AE measurements. Statistical analysis was performed using SPSS (v21.0, Microsoft, USA).

3 Results

There was no statistical difference in apparent density for bone samples among the five groups (**Table 2**).

3.1 AE measurements in compressive loading

Modulus reduction increased from group A to group E ($P < 0.001$) (**Table 2**). During compressive loading, AE hit occurred right before the ultimate load was reached and continued throughout the whole post-yield deformation stage (**Figure 3**). In compressive loading, AE measurements increased from group A to group E ($P < 0.05$) (**Table 2**).

3.2 Creep loading and AE measurements

All samples exhibited typical primary and secondary creep during the 30-min creep loading test before and after compressive loading (**Figure 4**). Tertiary creep, the stage after the primary and secondary creep, was observed in 2 samples (one in group B and another in group D) in the post-compressive loading creep test. For the one in group D (**Figure 5**), tertiary creep started at the 9th minute in the creep test and lasted for about 2 minutes. Then the sample started another secondary creep. Thus, creep rate was not calculated for this sample.

There was no statistically significant effect of donor on creep deformation ($P > 0.05$). Before compressive loading, creep deformation was not different among the five groups ($P > 0.05$). After compressive loading, creep deformation was significantly greater in group D and E than in other three groups ($P < 0.05$) (**Table 3**). In group E, the median value of creep strain (including primary and secondary creep) reached 1.6% at the end of creep loading.

Most AE hits occurred in the primary creep (**Figure 4**). AE hits were rare in the secondary creep either before or after compressive loading (only recorded in 7 samples, including 4 in group A and 3 in E, with 23 hits in total). Similar pattern was also observed for the sample in

group D which went into tertiary creep at 9th minute (**Figure 5**). While there were a lot of AE hits recorded in tertiary creep, very few AE hits were recorded in the secondary creep either before or after tertiary creep. Therefore, statistical analysis was only performed for AE measurements in the primary creep.

Before compressive loading, AE hits are rare during the primary creep and no difference in AE measurements was observed among the five groups (**Table 4**). After compressive loading, however, AE measurements during the primary creep were significantly different among the five groups ($P < 0.05$). All AE measurements in group E were significantly greater than those in group A, B, and C ($P < 0.05$ for all), while those in group D were significantly greater than those in group C ($P < 0.05$ for all). There was no statistical difference in AE measurements between group D and E.

The amount of creep strain was correlated to AE measurements during the primary creep ($\tau = 0.62, 0.62, 0.64, 0.59$ and 0.52 for cumulative hits, cumulative counts, cumulative duration, maximal amplitude, and mean amplitude, respectively, $P < 0.01$ for all). Creep rate in the secondary creep was correlated to AE measurements during the primary creep ($\tau = 0.60, 0.60, 0.58, 0.54$ and 0.50 for cumulative hits, cumulative counts, cumulative duration, maximal amplitude, and mean amplitude, respectively, $P < 0.01$ for all).

3.3 AE signal features in compressive loading and creep loading

In total, 275 AE hits were recorded during compressive loading and 95 hits in primary creep after compressive loading. AE signal features were similar between these two loading conditions. The median values of AE amplitude (50 dB) and duration (382 μ s) during compressive loading were not statistically different from that during second creep loading (51 dB and 400 μ s, respectively, $P > 0.05$, Mann-Whitney U test). There was no association

between the numbers of AE hits during compressive loading and during second creep loading
($\tau = 0.15$, $P > 0.05$).

4 Discussion

For the first time, AE technique was used to study creep behaviours in human vertebral trabecular bones. Creep behaviours of vertebral trabeculae depended on the degree of bone damage. With the increase of bone damage, substantial creep deformation can occur in the vertebral trabeculae even when the bone was under physiological loading. Findings provide a possible explanation as to why some patients with vertebral compression fracture developed progressive vertebral collapse and kyphosis over time.

4.1 Explanation of results

The substantially increased creep deformation occurred after the trabecular bones underwent post-ultimate strain compression. This may be related to new presentation of creep damage. During the primary creep, high-energy AE signals (amplitude > 50dB) were common in group D and E (**Table 4**). Interestingly, such high-energy AE signals were also recorded during compressive loading when post-yield deformation occurred, suggesting that these AE hits were produced by new damage in the bones. Previous studies also reported similar high energy AE signal when fracture was induced to trabeculae [18, 29, 30]. The bone damage in primary creep likely includes large microcracks or even trabeculae fracture [18, 30]. On the other hand, as creep rate in the secondary creep correlated to AE measurements in the primary creep, it is also possible that the bone damage occurred in the primary creep continued to evolve during the secondary creep, which may include formation of diffuse damage [3], slow growth of microcracks [31], and separation of fractured trabeculae. Support for this argument can be found in one of the two samples that went into tertiary creep (**Figure 5**). While only a few AE hits were recorded in the secondary creep (the first 8 minutes of the creep loading), a large amount of AE hits occurred when the tertiary creep starts, suggesting that continuous evolution of damage during secondary creep leads to

microcracks or fractures in vertebral trabeculae. Other techniques, such as high resolution micro-CT, may help to further answer this question.

The effect of trabecular bone damage on creep behaviours may relate to the loss of bone structural integrity. When the damaged trabecular bone underwent creep loading, stress distribution within the bone will be rearranged, resulting in stress concentration and new fracture in undamaged trabeculae [32, 33]. Evidence suggests that stress rearrangement depends on degree of bone damage [34]. Stress rearrangement in bone was negligible when modulus reduction was below 30%, but became significant if modulus reduction was greater than 30% [34]. This may explain why both AE measurements and creep deformation were significantly greater in group D and E where modulus reduction is above 30% but remained unchanged in group B and C where modulus reduction is below 30%.

4.2 Relationship to previous work

Results of the current experiments are comparable to previous findings that bone creep involves in viscoelastic and damage processes [6, 11, 12] which may lead to progressive deformity in human vertebrae [6, 7]. For the first time, this study used AE technique to study creep behaviours of vertebral trabeculae. Findings of this study suggested that the substantial creep deformation observed in group D and E may be a result of new trabecular microfractures or extension of existing microfractures.

4.3 Strength and limitation of the study

A strength of the current study is using AE technique to monitor vertebral damage accumulation in creep deformation. AE technique is highly sensitive and is able to detect crack as small as 25 μm in cortical bone in a fatigue test [16]. Moreover, this technique can demonstrate the time history of microdamage evolution and thus, provide important information for understanding the mechanism underlying bone creep. While the same

experiment protocol was used to test all samples, a fixed level of strain was employed in each group to induce equivalent amount of bone damage [25]. Such a study design may minimize experimental errors and confounding.

Although AE technique is sensitive, it is not able to detect bone microcracks less than 25 μm [16]. As such, some diffuse damages ($< 1 \mu\text{m}$) were missed [3]. Another study limitation is that creep tests were conducted at room temperature. As the creep rate increases at higher temperature [35], in vivo creep measurements should be greater than that observed in the current study. While full recovery of creep deformation may take much longer time than the loading time [11], a recovery period of 30 minutes in the current study is not enough to allow a full recovery. This may be one of the reasons why creep strain is lower in the second creep loading, as compared with the first one for groups A, B, and C (**Table 3**). The age range for samples studied is wide (36 to 73 years), resulting in a high variability in apparent density measurement and some bone samples may not be representative of that in osteoporosis. Although bone samples were heterogeneous, a constant stress of 0.4 MPa was used during creep loading. As such, elastic strains induced in bones may vary considerably. While damage of trabecular bone is dependent on strain [25], this approach may lead to high intra-group variability in creep deformation and AE measurements, as observed in the current study. In addition, in real life human vertebral trabecular bone are subjected to cyclic fatigue loading, which include both creep and cyclic loading. Although creep plays an important role in trabecular bone deformation in cyclic fatigue loading[11], we did not study cyclic loading. Finally, although the relationship of bone damage and creep deformation was identified in this experimental study, bone damage is merely quantified by a mechanical measure (modulus reduction) and how to reflect bone damage using standard image approaches remains unknown.

4.4 Clinical significance

Finding that with the increase of trabecular bone damage substantial creep deformation can occur provides a possible explanation as to why some cases of acute vertebral fractures will develop progressive vertebral collapse but some will not [3]. Healing of trabecular bone was found to be most efficient in a biomechanical environment with interfragmentary strain ranged between 6% and 20%. Healing will be delayed when cyclic strain was either too low (<5%) or too high (>20%) [36]. Substantial creep deformation may disturb and delay bone healing, and even initiate a vicious cycle of progressive vertebral collapse and deformity [4]. Findings may also contribute to new screening tools to identify patients at risk of progressive vertebral collapse, though such a clinically feasible tool remains to be developed.

Funding: This work was supported by a grant from Sir Halley Stewart Trust, UK

References

- [1] Johnell O, Kanis JA. An estimate of the worldwide prevalence and disability associated with osteoporotic fractures. *Osteoporos Int* 2006;17: 1726-33.
- [2] Kendler DL, Bauer DC, Davison KS, Dian L, Hanley DA, Harris ST, McClung MR, Miller PD, Schousboe JT, Yuen CK, Lewiecki EM. Vertebral Fractures: Clinical Importance and Management. *Am J Med* 2016;129: 221 e1-10.
- [3] Ito Y, Hasegawa Y, Toda K, Nakahara S. Pathogenesis and diagnosis of delayed vertebral collapse resulting from osteoporotic spinal fracture. *Spine J* 2002;2: 101-6.
- [4] Baba H, Maezawa Y, Kamitani K, Furusawa N, Imura S, Tomita K. Osteoporotic vertebral collapse with late neurological complications. *Paraplegia* 1995;33: 281-9.
- [5] Goldstein S, Smorgick Y, Mirovsky Y, Anekstein Y, Blecher R, Tal S. Clinical and radiological factors affecting progressive collapse of acute osteoporotic compression spinal fractures. *J Clin Neurosci* 2016;31: 122-6.
- [6] Pollintine P, Luo J, Offa-Jones B, Dolan P, Adams MA. Bone creep can cause progressive vertebral deformity. *Bone* 2009;45: 466-72.
- [7] Luo J, Pollintine P, Gomm E, Dolan P, Adams MA. Vertebral deformity arising from an accelerated "creep" mechanism. *Eur Spine J* 2012;21: 1684-1691.
- [8] Kim DG, Shertok D, Ching Tee B, Yeni YN. Variability of tissue mineral density can determine physiological creep of human vertebral cancellous bone. *J Biomech* 2011.
- [9] Kopperdahl DL, Pearlman JL, Keaveny TM. Biomechanical consequences of an isolated overload on the human vertebral body. *J Orthop Res* 2000;18: 685-90.
- [10] Manda K, Wallace RJ, Xie S, Levrero-Florencio F, Pankaj P. Nonlinear viscoelastic characterization of bovine trabecular bone. *Biomech Model Mechanobiol* 2016.

- [11] Yamamoto E, Paul Crawford R, Chan DD, Keaveny TM. Development of residual strains in human vertebral trabecular bone after prolonged static and cyclic loading at low load levels. *J Biomech* 2006;39: 1812-8.
- [12] Fondrk M, Bahniuk E, Davy DT, Michaels C. Some viscoplastic characteristics of bovine and human cortical bone. *J Biomech* 1988;21: 623-30.
- [13] Hanagud S, Clinton RG. Acoustic emission techniques in the development of a diagnostic tool for osteoporosis. In: *IEEE symposium on ultrasonic*; 1975. p. 41-45.
- [14] Wright TM, Vosburgh F, Burstein AH. Permanent deformation of compact bone monitored by acoustic emission. *J Biomech* 1981;14: 405-9.
- [15] Agcaoglu S, Akkus O. Acoustic emission based monitoring of the microdamage evolution during fatigue of human cortical bone. *J Biomech Eng* 2013;135: 81005.
- [16] Rajachar RM, Chow DL, Curtis CE, N.A. W, Kohn DH. Use of acoustic emission to characterize focal and diffuse microdamage in bone. In: Vahavidos SJ, editor. *Acoustic emission: standards and technology update*. Philadelphia, PA: American Society for Testing and Materials (ASTM); 1999, p. 3-21.
- [17] Hasegawa K, Takahashi H, Koga Y, Kawashima T, Hara T, Tanabe Y, Tanaka S. Failure characteristics of osteoporotic vertebral bodies monitored by acoustic emission. *Spine (Phila Pa 1976)* 1993;18: 2314-20.
- [18] Wells JG, Rawlings RD. Acoustic emission and mechanical properties of trabecular bone. *Biomaterials* 1985;6: 218-24.
- [19] Keaveny TM, Pinilla TP, Crawford RP, Kopperdahl DL, Lou A. Systematic and random errors in compression testing of trabecular bone. *J Orthop Res* 1997;15: 101-10.
- [20] Keaveny TM, Guo XE, Wachtel EF, McMahon TA, Hayes WC. Trabecular bone exhibits fully linear elastic behavior and yields at low strains. *J Biomech* 1994;27: 1127-36.
- [21] ASTM. *ASTM E650 / E650M-12 Standard Guide for Mounting Piezoelectric Acoustic Emission Sensors*. In. West Conshohocken, PA, USA: ASTM International; 2012.

- [22] ASTM. E976-10 Standard guide for determining the reproducibility of acoustic emission sensor response. In. West Conshohocken, PA, USA: ASTM International; 2010.
- [23] Van Toen C, Street J, Oxland TR, Cripton PA. Acoustic emission signals can discriminate between compressive bone fractures and tensile ligament injuries in the spine during dynamic loading. *J Biomech* 2012;45: 1643-9.
- [24] Sato K, Kikuchi S, Yonezawa T. In vivo intradiscal pressure measurement in healthy individuals and in patients with ongoing back problems. *Spine (Phila Pa 1976)* 1999;24: 2468-74.
- [25] Wachtel EF, Keaveny TM. Dependence of trabecular damage on mechanical strain. *J Orthop Res* 1997;15: 781-7.
- [26] Manda K, Xie S, Wallace RJ, Levrero-Florencio F, Pankaj P. Linear viscoelasticity - bone volume fraction relationships of bovine trabecular bone. *Biomech Model Mechanobiol* 2016.
- [27] Keaveny TM, Wachtel EF, Ford CM, Hayes WC. Differences between the tensile and compressive strengths of bovine tibial trabecular bone depend on modulus. *J Biomech* 1994;27: 1137-46.
- [28] Keaveny TM, Wachtel EF, Kopperdahl DL. Mechanical behavior of human trabecular bone after overloading. *J Orthop Res* 1999;17: 346-53.
- [29] Thomas IM, Evans JH. Acoustic emission from vertebral bodies. *Journal of Materials Science Letters* 1988;7: 267-269.
- [30] Leichter I, Bivas A, Margulies JY, Roman I, Simkin A. Acoustic emission from trabecular bone during mechanical testing: the effect of osteoporosis and osteoarthritis. *Proc Inst Mech Eng H* 1990;204: 123-7.
- [31] Hazenberg JG, Taylor D, Clive Lee T. Mechanisms of short crack growth at constant stress in bone. *Biomaterials* 2006;27: 2114-22.
- [32] Lifshitz JM, Rotem A. Time-dependent longitudinal strength of unidirectional fibrous composites. *Fibre science and technology* 1970;3: 1-20.

- [33] Nagaraja S, Ball MD, Guldberg RE. Time-dependent damage accumulation under stress relaxation testing of bovine trabecular bone. *International Journal of Fatigue* 2007;29: 1034-1038.
- [34] Luo Q, Leng H, Acuna R, Dong XN, Rong Q, Wang X. Constitutive relationship of tissue behavior with damage accumulation of human cortical bone. *J Biomech* 2010;43: 2356-61.
- [35] Bowman SM, Guo XE, Cheng DW, Keaveny TM, Gibson LJ, Hayes WC, McMahon TA. Creep contributes to the fatigue behavior of bovine trabecular bone. *J Biomech Eng* 1998;120: 647-54.
- [36] Claes L, Reusch M, Gockelmann M, Ohnmacht M, Wehner T, Amling M, Beil FT, Ignatius A. Metaphyseal fracture healing follows similar biomechanical rules as diaphyseal healing. *J Orthop Res* 2011;29: 425-32.

Figure Legends

Figure 1. Setup of mechanical testing apparatus (A, compression plate; B, bone sample; C, testing chamber; D, acoustic emission sensor).

Figure 2. Signal features of an AE hit. An AE threshold was set to eliminate false triggers from noise. Features of AE signal, including amplitude, count, and duration were acquired using AEWIn software.

Figure 3. Stress and cumulative AE hits during compressive loading test.

Figure 4. Creep strain and cumulative AE hits during second creep test for a sample in group E. In the primary creep (T1), creep strain increased rapidly and most AE hits occurred during this period. In the followed secondary creep (T2), the creep strain increased at a much lower rate.

Figure 5. Creep strain and cumulative AE hits for a sample in group D. The sample went into tertiary creep at 9th min during creep loading. Both creep strain and AE hits increased rapidly during tertiary creep. The tertiary creep lasted for around 2 minutes, after which the sample started another secondary creep.

Table 1. Details of cadaveric spines in the study

Cadaveric spine	Donor information		Vertebrae dissected	Vertebrae used in this study
	Age	Sex		
1	73	M	L1-L5	L2, L4
2	55	M	T9-L5	T10-L5
3	36	F	T8-L5	T8, T11, L1-L4
4	64	F	T8-L5	T10, L2, L4
5	56	M	T8-L4	T12, L2

Table 2. Apparent density, modulus reduction and AE measurements during compressive loading

Measurements	Group					P
	A	B	C	D	E	
Apparent density (g/cm ³)	0.23 ± 0.08	0.24 ± 0.11	0.26 ± 0.09	0.24 ± 0.04	0.32 ± 0.09	0.324
Modulus reduction (%)	-3.73±10.47	5.49±27.69	26.11±24.63	65.57±11.12	78.29±13.30	<0.001
Cumulative hits	0(3)	1(4)	4(8)	10(15)	31(29)	<0.001
Cumulative counts	0(107)	19(61)	128(355)	399(520)	1140(840)	<0.001
Cumulative duration (ms)	0(1.39)	0.50(1.99)	2.03(5.34)	3.75(7.68)	14.37(10.57)	<0.001
Maximal amplitude (dB)	0(55)	47(56)	60(36)	69(25)	78(7)	<0.001
Mean amplitude (dB)	0(51)	43(48)	50(13)	52(8)	53(4)	0.004

Data are mean ± SD for apparent density and modulus reduction, and median (IRQ) for the others. P values indicate the difference across the five groups (one-way ANOVA for apparent density and modulus reduction, and Kruskal-Wallis test for the others).

Table 3. Creep strain during primary creep and creep rate during secondary creep measured pre- and post- compressive loading

		Group					P
		A	B	C	D	E	
Creep strain (μ strain)	Pre-	1631(6742)	2280(4683)	1818(653)	2176(7009)	1610(2246)	0.696
	Post-	544(628) ^{DE}	598(3745) ^{dE}	985(607) ^{DE}	6022(13359)	13593(79865)	<0.001
Creep rate (μ strain/s $\times 10^{-4}$)	Pre-	3107(9400)	4374(4500)	3577(900)	3817(3500)	3137(1500)	0.291
	Post-	1942(1600) ^{dE}	2427(2600) ^e	1891(1200) ^{dE}	8210(18500)	14815(40800)	0.001

Data are median (IRQ). P values indicate the difference among the five groups (Kruskal-Wallis test). When compared with group E, statistical differences were denoted with ^e if $P < 0.05$ and ^E if $P < 0.01$, and those compared with group D were denoted with ^d if $P < 0.05$ and ^D if $P < 0.01$ (Mann-Whitney U test).

Table 4. AE measurements during primary creep pre- and post- compressive loading

AE parameter		Group					P
		A	B	C	D	E	
Cumulative hits	Pre-	1(2)	0(3)	0(3)	3(9)	0(0)	0.227
	Post-	0(1) ^E	0(2) ^E	0(0) ^{dE}	3(7)	6(16)	0.002
Cumulative counts	Pre-	7(94)	0(108)	0(150)	54(265)	0(0)	0.282
	Post-	0(13) ^E	0(84) ^E	0(0) ^{dE}	100(281)	157(779)	0.002
Cumulative duration (ms)	Pre-	0.02(0.95)	0(1.83)	0(1.42)	1.15(3.77)	0(0)	0.250
	Post-	0(0.04) ^E	0(0.85) ^E	0(0) ^{dE}	0.93(2.93)	1.97(7.15)	0.002
Maximal amplitude (dB)	Pre-	48(59)	0(40)	0(51)	52(55)	0(0)	0.227
	Post-	0(23) ^E	0(38) ^e	0(0) ^{dE}	55(63)	66(19)	0.004
Mean amplitude (dB)	Pre-	47(54)	0(37)	0(47)	47(49)	0(0)	0.220
	Post-	0(23) ^e	0(37) ^e	0(0) ^{dE}	49(52)	54(6)	0.008

Data are median (IRQ). P values indicate the difference among the five groups (Kruskal-Wallis test). When compared with group E, statistical differences were denoted with ^e if P<0.05 and ^E if P<0.01; those compared with group D were denoted with ^d if P<0.05 and ^D if P<0.01 (Mann-Whitney U test).

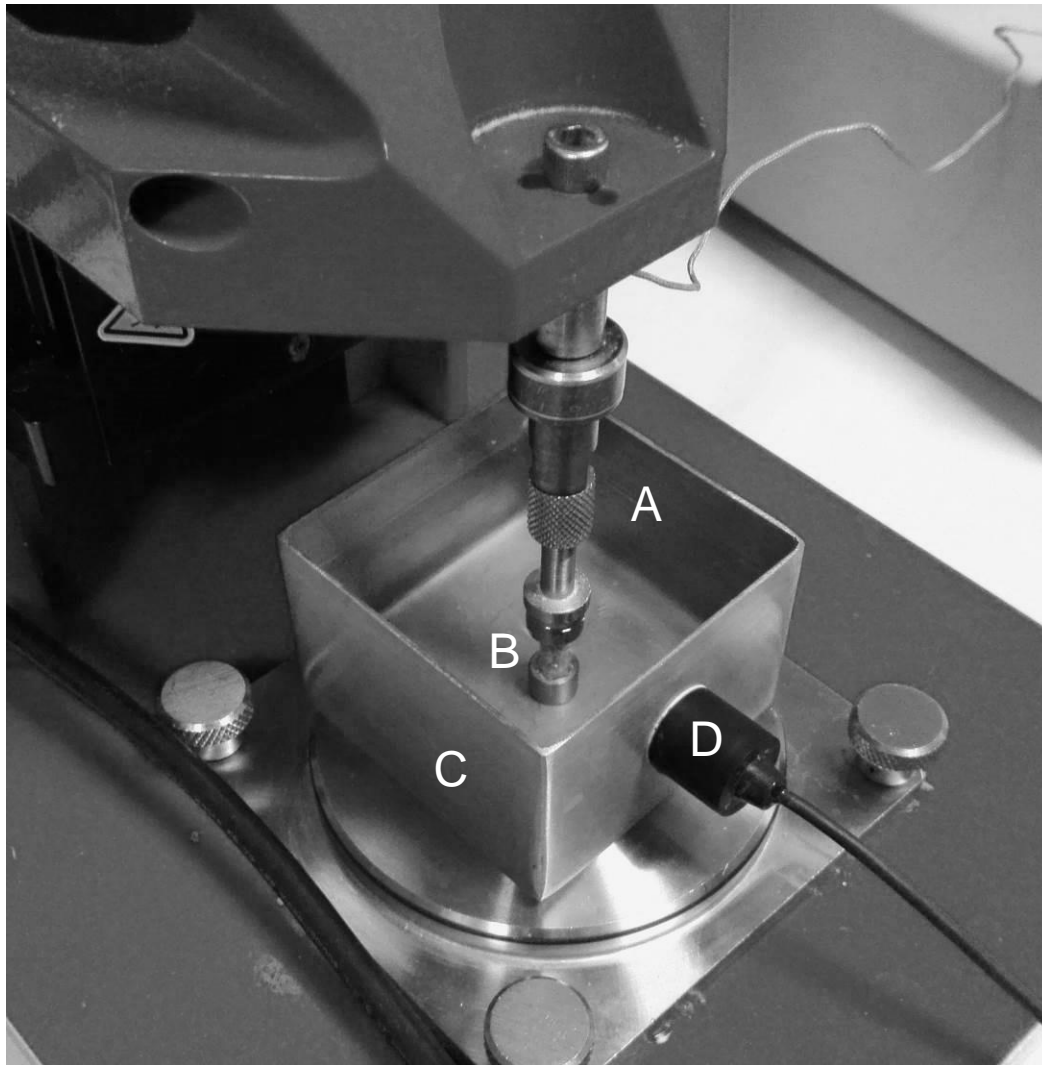


Figure 1

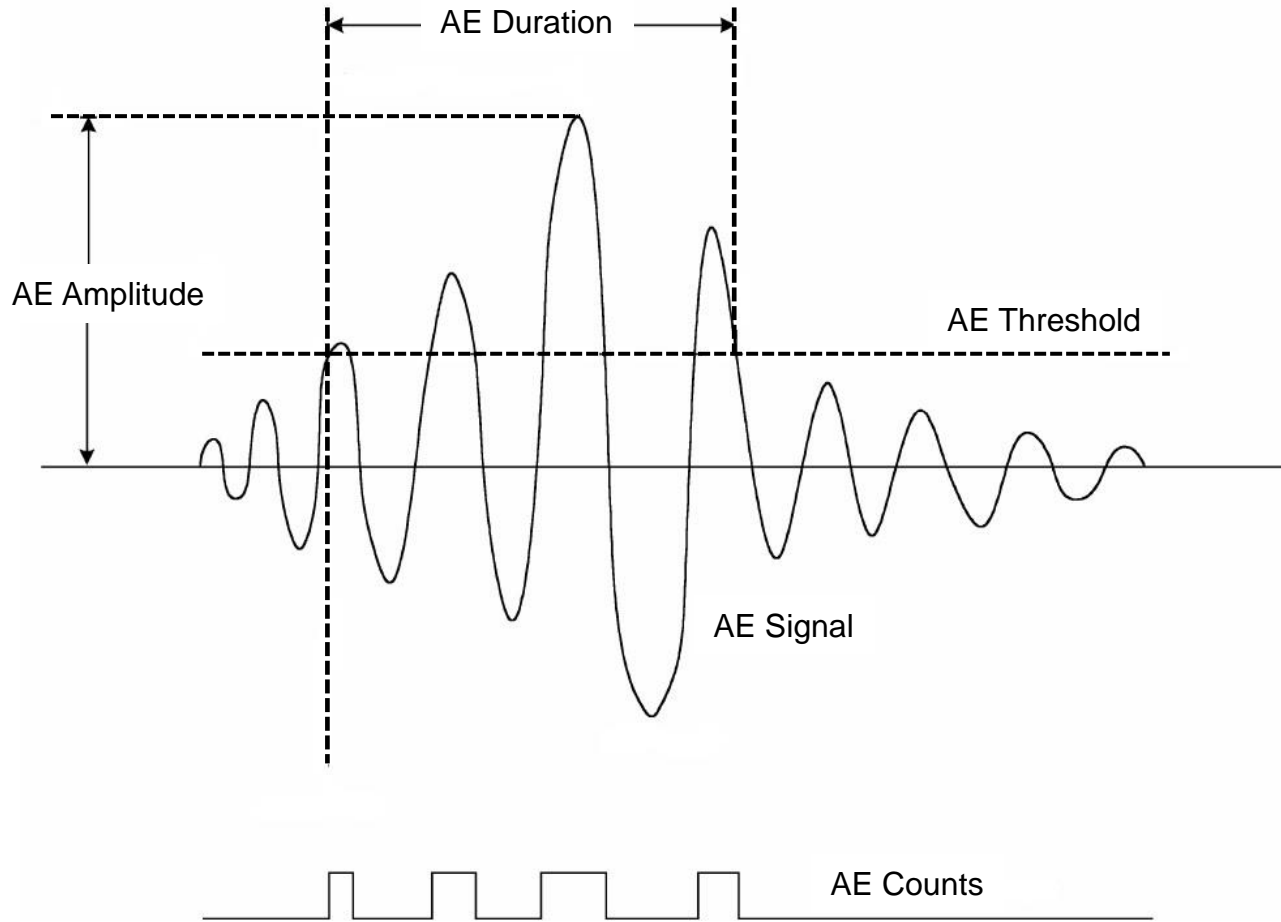


Figure 2

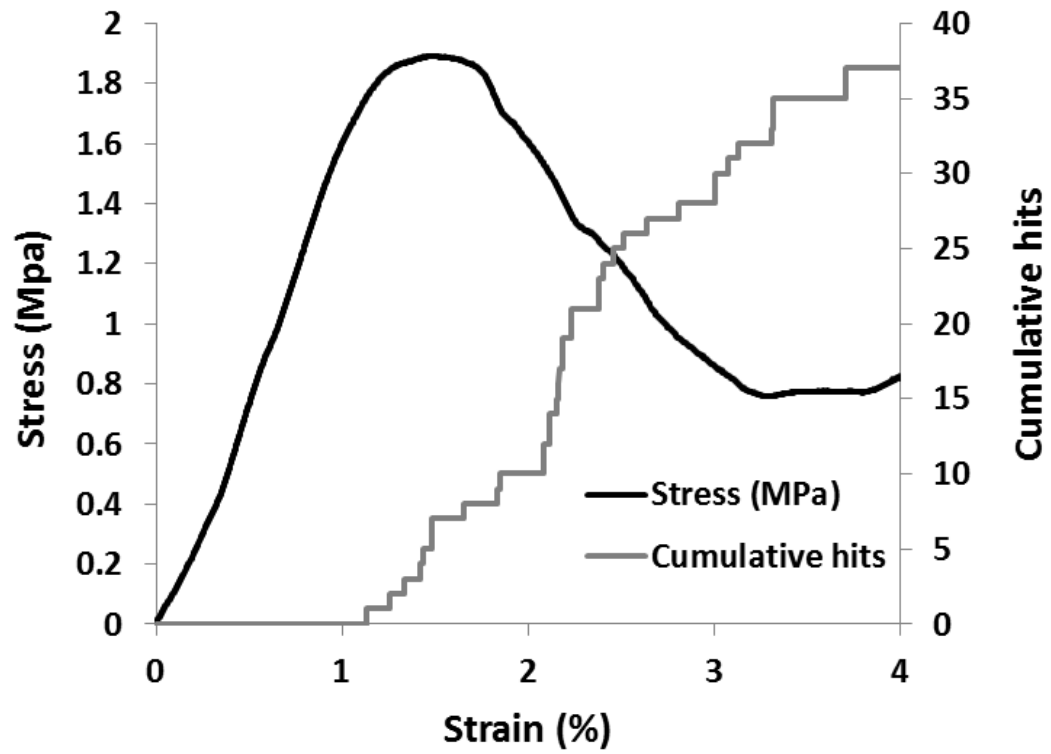


Figure 3

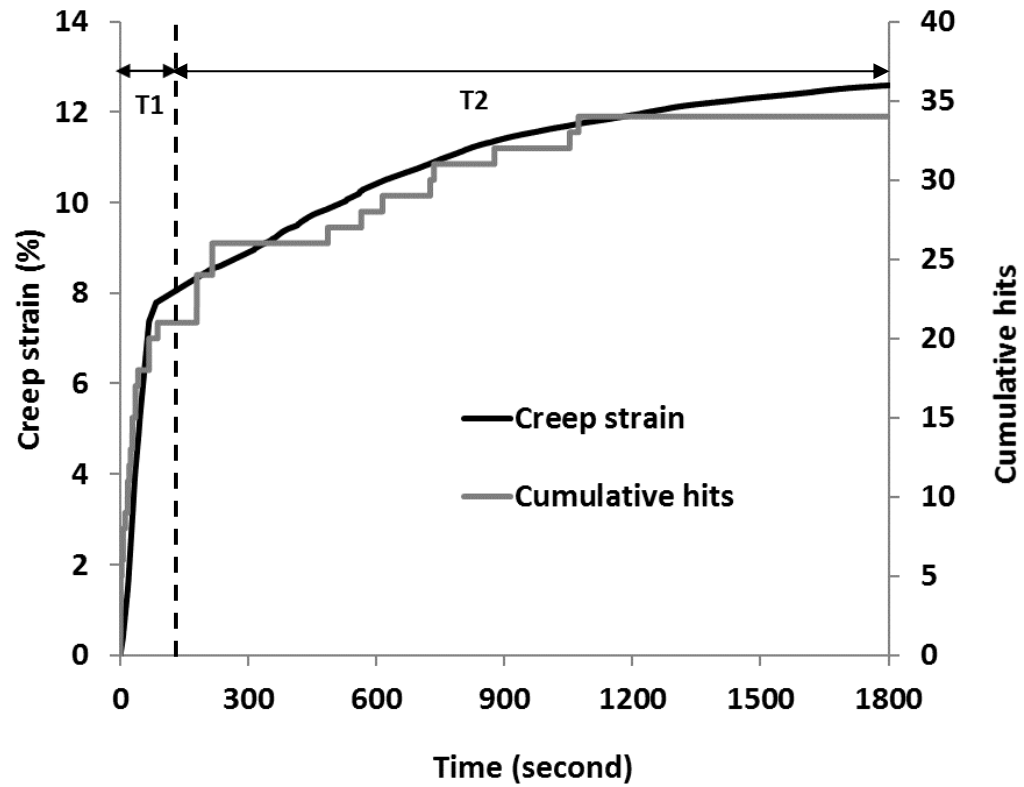


Figure 4

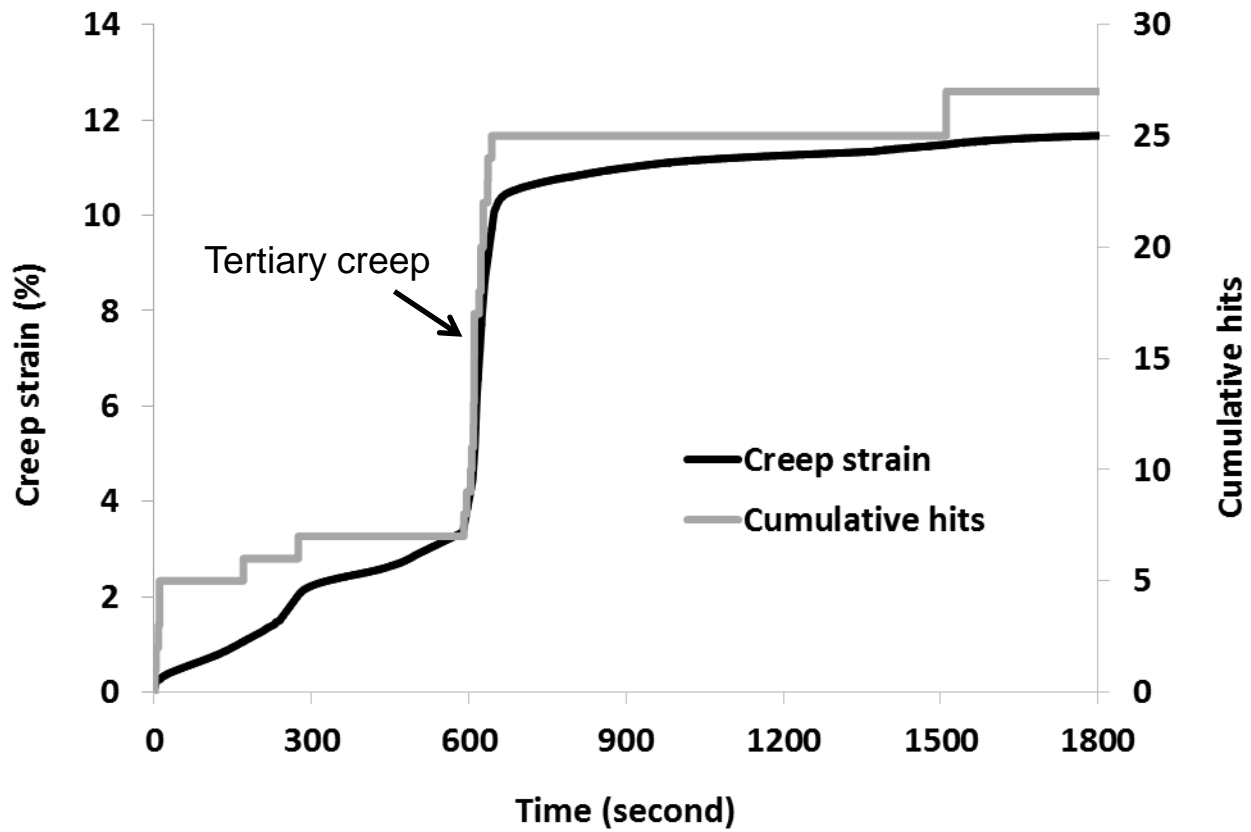


Figure 5